UNSTEADY THREE-DIMENSIONAL SIMULATIONS OF VTOL UPWASH FOUNTAIN TURBULENCE

Robert E. Childs and David Nixon
Nielsen Engineering & Research, Inc.
Mountain View, CA 94043

ABSTRACT

Numerical simulations of a planar turbulent wall jet and a planar VTOL upwash fountain have been performed. These are three-dimensional simulations and they resolve large scale unsteady motions in the flows. The wall jet simulation shows good agreement with experimental data and is presented to verify the simulation methodology. Simulation of the upwash fountain predicts elevated shear stress and a half-velocity width spreading rate of 33% which agrees well with experiment. Turbulence mechanisms which contribute to the enhanced spreading rate are examined.

1. INTRODUCTION

The desire to have a VTOL supersonic fighter has increased in recent years as there are many advantages in having an aircraft that can be based independent of conventional runways. VTOL capability is provided by some combination of downward thrusting jets. In ground effect these jets produce fluid dynamical problems that are not typically encountered in conventional aircraft. A complete list of ground effects problems would be rather large and would include, for example, the Reynolds number scaling of the "suck-down" effect, the enhanced spreading rate of the upwash fountain, hot gas reingestion of the fountain or ground vortex fluid, and aircraft stability problems due to interaction with the fountain or the ground vortex.

The key to an understanding and a predictive capability in many of the above problems is in the ability to understand the turbulent mixing. The suck-down effect and the fountain's spreading rate are almost purely turbulence problems; the ground vortex also depends on inviscid and bouyancy phenomena. These are complex turbulent flows, involving combinations of "turbulence modifiers" that are rarely encountered in other applications and, therefore, it will be difficult to develop adequate models for these flows.

This paper focuses on the turbulence in the upwash fountain, sketched in Figure 1, which is important for several practical reasons. The upwash is hot, it strikes the underside of the aircraft, it contributes to lift, and it may lead to exhaust gas reingestion. From a scientific standpoint the upwash spreading rate is an anomaly which begs to be explained. The combination of streamline curvature and velocity gradient can have a pronounced effect on turbulent mixing [Refs. 1, 2, 3]. Present understanding indicates that the combination of curvature and velocity gradient, like that in a boundary layer on a convex surface, should stabilize the turbulence in most of the turning region of the fountain. However, just the opposite occurs and the shear stresses and spreading rate are two to three times greater than in a conventional jet. There is a near-wall region which has shear of the opposite sign, and for which the curvature-velocity gradient combination effect should be destabilizing. This region is small in the wall jets and in the fountain, but in the collision zone it encompasses much of the reversed-flow zone under the fountain. However, it seems unlikely that this relatively small region of the flow could energize the turbulence in all of the fountain.

The high stresses and spreading rate are underpredicted by most classes of current turbulence models: the k-ε, the algebraic Reynolds stress, and the Reynolds stress transport models [Ref. 4 and Launder, private communication]. These models seem to be insensitive to the turbulence mechanisms in the fountain's turning region. For obvious reasons it is desirable to have a model that gives improved results for this flow. Additionally, it is clear that these potentially significant mechanisms are not represented in the modeling of other flows, where their absence, not being as critical, has escaped detection. The essential feature of the upwash fountain is colliding wall-bounded shear layers with strong curvature at the collision point. A two-dimensional boundary layer with a reversed flow region has similar features at the separation point.

Finally, it is worth noting that experimental studies of the fountain are difficult to perform. The flow is highly unsteady with frequent flow direction reversal in the critical region where the wall jets collide. Laser instrumentation would seem to be necessary for this work, but has only recently been employed [Ref. 6]. Furthermore, the large pressure gradients in a region of unsteadiness indicate that pressure fluctuations may be important and these cannot be measured at present. The pressure-strain term in the Reynolds stress transport equations has, therefore, not been directly measured although it is thought to be important in curved flows.

1.1 The Approach

In this work two flows are simulated, the planar wall jet, chosen because it is a well documented flow which can be used to validate the numerical method, and the planar upwash fountain. There are many advantages to studying the planar flow rather than the fountain resulting from radial wall jets, which more closely resembles the VTOL ground effect flow field. These include the ability to use periodic boundary conditions in one direction and shorter computing times for good statistics.

The simulations are done by specifying unsteady inflow conditions that approximate the turbulent wall jets. These flows then evolve in the streamwise direction before they are evaluated, in the case of the wall jet simulation, or collide with another wall jet, in the fountain simulation. Instantaneous and time-averaged data are obtained from the simulation. This makes the work similar to an experimental program except that the type and quantity of data available can be greater. To date single point correlations of velocities, velocity gradients, pressure and density have been obtained. These terms give us, from the Reynolds-averaged standpoint, the ability to determine most of the mechanisms critical to the turbulence in the fountain. This work is similar to the work in Large Eddy Simulation (LES) reviewed by Rogallo and Moin [Ref. 7], for example. Many differences distinguish LES from the present effort, which we call Very Large Eddy Simulation (VLES).

2. METHODS

2.1 Equation Set and Numerical Algorithm

The simulations have been performed using a conventional finite difference method that is often used for steady-state Reynolds-averaged calculations of aerodynamics problems. The viscous conservation equations for mass, energy, and momenta in three directions (commonly, the Navier-Stokes equations) are used for the simulations. They are written in a conservation law form common for high speed aerodynamics. The solution algorithm is the 1981 implicit-explicit MacCormack method [Ref. 8]. The implementation of the algorithm includes modifications to improve its efficiency for this application; these are discussed in Childs and Nixon [Ref. 5]. The two significant modifications are: 1) viscous diffusion terms are first order in time, as opposed to the second order accuracy of the original algorithm (not a significant disadvantage since the sub-grid-scale turbulence model, which dominates viscous diffusion, has no formal accuracy at all, and convective terms are still second order in space and time); and 2) the time step is chosen such that the algorithm is explicit in the two directions parallel to the wall. The implicit step is only used normal to the wall. Due to the grids which are used the algorithm is entirely explicit away from the grid clustering at the wall. This minimizes the dissipative effects of an implicit method, but does not overly restrict the time step.

The difficulty at solid boundaries with the 1981 MacCormack method [Ref. 9] has not been a problem in the present work since the time steps needed to resolve the turbulence are relatively small and give a maximum CFL number of 20, typically.

The simulations are performed on rather coarse grids because of computer limitations and only the largest scales of turbulence can be simulated. Therefore, the equations are Reynolds-averaged and a sub-grid-scale (SGS) model is used for the unresolvable scales of turbulence which, it is assumed, are more easily modeled and less critical to the turbulent processes than the large scales. We use an eddy viscosity which is proportional to the magnitude of vorticity

$$\nu_t = C\Delta^2 \sqrt{\omega_i \omega_i} \qquad (1)$$

The value of $C\Delta^2$ represents the square of the SGS mixing length. A constant characteristic grid spacing Δ is used, since the grid spacing in the x- and z-directions is nearly constant in the collision zone. The coefficient C takes the value of $C = 0.14$ which is close to the values used for LES in References 10 and 11, except near the wall. At the wall C approaches zero according to the Von Karman formula so that the log-law profile is reproduced.

2.2 Boundary Conditions

There are several types of boundary conditions which must be applied in these simulations. The straight-forward ones will be discussed first, then the more difficult inflow and outflow conditions will be given.

In the z-direction the flow is periodic. This condition is imposed by over-writing the boundary points with data from the first interior point at the opposite side of the grid. At the solid wall the no-slip condition is applied to velocities and a zero-gradient condition is applied to the density and energy. The wall falls between two grid points and these conditions imply a zero-gradient on temperature and pressure.

At the top of the domain there is outflow in the fountain and slow flow, either in or out, on either side of the fountain. This boundary is treated with a zero-gradient extrapolation condition on all variables. There is no effort to obtain meaningful data at this boundary. The primary concern is that there be no reflection of pressure waves. From analysis of outflow boundary conditions (c.f. Ref. 12) the imposition of pressure and extrapolation of density and velocities is correct for steady calculations. However, imposing a pressure at the top would produce pressure reflections.

The side boundaries above the wall jets must provide a small amount of inflow for entrainment into the jet. It would be incorrect to specify the inflow because that could amount to specifying the entrainment into the jet. A zero-gradient condition on the velocities permits the inflow to adjust as necessary to satisfy the entrainment. The density is set to ambient. At some point the pressure must be tied to ambient conditions and there is no other suitable place to do this since all other boundaries will experience significant pressure fluctuations. A "loosely tied pressure" condition is used, which provides a small "pull" towards ambient pressure, but permits the pressure to deviate if the interior flow so requires. The loosely tied pressure is computed as a weighted average of the local interior pressure and the fixed ambient pressure. Typically the weighting is about 30% on the ambient pressure and 70% on the interior pressure. A similar type of pressure

boundary condition was used by Boris [Ref. 13] in the simulation of turbulent outflow.

The inflow conditions are clearly the most difficult. They must approximate the mean and turbulent flow in a fully developed turbulent wall jet. There were two guiding principles used in determining the inflow. Firstly, it should give correct values for the mean flow and basic statistics, the normal and shear stresses. Secondly, the unsteady inflow should "look right" when compared to flow visualization pictures. A third condition, on the turbulent energy spectrum, may be examined in the future.

The unsteady inflow profiles are constructed from a combination of Chebyshev modes normal to the wall and Fourier modes in the z-direction and time. This is added to a mean inflow profile determined from experimental data [Ref. 14, p. 434]. The following expression gives the unsteady streamwise velocity perturbation

$$u'(y,z,t) = \overline{U}_{max} \sum_{\ell,m} \alpha_{\ell,m} T_m(y) \sin(\omega_\ell z \pm c_\ell t) \qquad (2)$$

The Chebyshev polynomials are represented by $T_m(y)$. The ω_ℓ are wavelengths, the c_ℓ are wave speeds and the $\alpha_{\ell,m}$ are weighting coefficients. The lateral and vertical components are specified as functions of the streamwise fluctuations.

$$\begin{aligned} v' &= u' [\pm \beta_1 + \beta_2 \sin(\omega_p z) \sin(t)] \\ w' &= u' [\quad \beta_3 \sin(\omega_p z) \sin(t)] \end{aligned} \qquad (3)$$

The many coefficients in Equations (2) and (3) must satisfy certain constraints. The velocity perturbation goes to zero at the wall and the edge of the jet, and the maximum values of the normal and shear stresses must agree with experiment. These conditions do not uniquely determine the coefficients and the condition on the "appearance" of the unsteady profile was employed to determine ratios between some coefficients. The inflow density was set to ambient and the pressure was extrapolated from the interior. Specification of the above boundary conditions completes the description of the method.

2.3 Grids, Statistics and Computation Times

Cartesian grids with stretching in the x- and y-directions are used. The grid is clustered at the wall and in the center of the domain (for upwash simulations) where the fountain is expected to form. Simulations have been run on two grids with different resolutions for both the wall jet and the fountain. The results showed grid dependence in magnitude but not in character; in particular, the spreading rate of the fountain was very similar in both cases. The finer grid results are shown. For the fountain the grid has 40 by 32 by 25 points in the x, y, and z directions; for the wall jet the grid has 32 by 32 by 32 points.

Analysis of the turbulence is done by accumulating single point statistics of velocities, velocity gradients, pressure, density and energy. These are then processed to provide the turbulent correlations. The flow is two-dimensional in the mean and statistical averaging is done over time and the z-direction, which is the mean-invariant direction. Turbulence evaluation is based on the assumption of constant density, which is sufficiently accurate for the present purposes.

The integration times are, so far, marginally adequate for some correlations, which are still changing slowly with time. Second order correlations, which give the Reynolds stresses and pressure-strain terms, appear to be stable to within 5% for the wall jet simulation but variations of 20% may be seen in the fountain results. Higher order statistics are not sufficiently converged for many purposes. Variations of 50% may be seen before they stabilize. The reason is that higher order statistics are formed from small differences between lower order statistics. Small variations in the lower order statistics can produce large changes in the higher order correlation. The higher order statistics are given to show orders of magnitude and trends, which are firmly established.

These calculations have been run on a CRAY X-MP. The upwash fountain was run for 90 minutes of CPU time and statistics were taken over the last 45 minutes. This provided 110 units of physical time nondimensionalized on the acoustic speed and initial wall jet half-velocity thickness, or approximately 1.7 "flow-through" time periods (time for the maximum-velocity fluid to transit the domain).

3. RESULTS

The results will be presented in two stages. The first step is to validate the simulation, which is done for the wall jet. The accuracy of the wall jet simulation will indicate what accuracy can be expected for the fountain simulation. The second stage is to examine the results for the fountain and investigate the turbulence mechanisms.

3.1 The Wall Jet

The simulation is of a two-dimensional wall jet on a plane surface with no streamwise pressure gradient. The calculation was run with a mean maximum inflow Mach number of 0.65, which is slow enough to minimize compressibility effects yet fast enough to maintain good computational efficiency. The wall and the "freestream" were given a velocity of 10% of the inflow maximum. This gives clearly defined inflow and outflow boundaries. Since the freestream and wall have the same velocity the flow has the conditions required for self-preservation. The added velocity is removed from all data analysis and the results. The Reynolds number based on maximum velocity, U_m, and half-velocity thickness, $y_{1/2}$, is 20000. The data to be used for comparison were compiled by Launder and Rodi for the 1980-81 Stanford-AFOSR

Conference [Ref. 14] from several experiments referenced therein.

For the comparison we use time-averaged results from the unsteady simulation. Figure 2 gives the velocity vectors at every fourth streamwise grid line. The dimensions in all two-dimensional figures are normalized on the half-velocity thickness at the inlet. The inlet velocity profile is specified to match experimental data. Between x=1 and x=9 the profile departs from experiment and shows a velocity profile which is too steep in the outer third of the jet. By x=10 the velocity profile is once more in agreement with experiment, as shown in Figure 3. There are small errors near the wall, but this is where the grid resolution in the x- and z-directions is the poorest relative to the need, and most of the shear stress is carried by the SGS model. The growth rate of the half-velocity thickness (at x=10) is 0.067, which is 9% below the experimental value of 0.073. Although the mean velocity profile has stabilized at this point, many of the turbulent statistics have not. The flow is not yet self-preserving.

In Figure 4 the resolvable components of the normal stresses are given. Clearly, the SGS contribution to the stresses should be positive (which eddy viscosity models don't guarantee) and, thus, the total stresses would be greater than the values shown. The resolvable stresses are all within 20% of the experiment and predict the trends that are important, including the slight rise in the u' and w' near the wall. The reduction in u' and w' very near the wall is physically correct behavior, although the region where this occurs is too thick in the simulation. This is likely caused by inadequate numerical resolution, but may also be due to the SGS model.

The resolvable and resolvable-plus-SGS shear stresses are shown in Figure 5. Consider first only the resolvable stress. The stress in the outer 75% of the wall jet is well predicted, although the location and magnitude of stress at its maximum are slightly high. In the near-wall region the stress is badly underpredicted. Considering the poor resolution here this problem was not unexpected. When the SGS stress is included, the near-wall results improve and give nearly the correct skin friction. However, the stress in the outer layer is now overpredicted by about 60%.

Figure 6 gives the triple velocity correlations of $\overline{u'u'u'}$, $\overline{u'v'v'}$ and $\overline{v'v'v'}$. These terms are responsible for the turbulent transport of the Reynolds stresses. They are important to understanding the turbulence, to multi-equation models, and to validating the present simulations. The results show that, in general, the trends and orders of magnitude are well predicted, with the exception that the near-wall region of $\overline{v'v'v'}$ is not. The overprediction of $\overline{u'u'u'}$ in the outer layer is consistent with the overprediction there of $\overline{u'u'}$. The prediction of $\overline{u'v'v'}$ (shear stress transport) is the best of the three and is only in significant error in the near-wall region. It should be noted that measurement errors of triple products are of the order of 15% to 30%, under the best conditions.

In summary for the wall jet the following are the major points. The resolvable normal stresses are predicted to within 20% of experiment, with the streamwise fluctuations being high and the vertical fluctuations being low. The shear stress in the outer layer is overpredicted by a significant amount. We do not believe this error will degrade the fountain simulation, for two reasons. In the fountain simulation the grid resolution of the wall jets is less and the turbulence levels are lower than in the pure wall jet simulation. Elevated turbulence in the fountain is, more than ever, due to mechanisms in the collision zone. Also, the turbulence levels in the fountain are many times greater than in the wall jet, so the turbulence production in the collision zone over-powers the wall jet turbulence. The third order correlations are adequate away from the wall, but are underpredicted in the near-wall region, which is due primarily to inadequate grid resolution in the x- and z-directions. In general, the turbulence in the wall jet is sufficiently close to experiment to permit useful study of the upwash turbulence.

3.2 The Upwash Fountain

The objective of this study is to examine the turbulence in the upwash fountain. The simulation was run by colliding two turbulent wall jets and permitting the upwash to develop naturally. The wall jets are run with the same inlet conditions as the pure wall jet.

For a point of comparison, the results from a steady state Reynolds-averaged calculation using a k-ε model are given in Figure 7. Although not shown, the turbulence levels and spreading rate are typical for the values seen in a "normal" free jet, and significantly underpredict the values seen in upwash fountains.

Figure 8 gives the mean velocity vectors and Mach number contours from the unsteady simulation, similar to Figure 7 from the steady calculation. Rapid spreading of the fountain is clearly seen. Initially a velocity deficit at the center of the fountain is seen but it quickly disappears above the collision zone. Streamlines, shown in Figure 8-c, reveal a two stage collision process. First the wall jets separate and flow over relatively large reversed flow regions. Then they collide above the separation zone and are redirected upward. The half velocity width of the fountain is plotted in Figure 9; it grows at a rate of 33% just above the collision zone. This compares well with experimental values in the range of 24% to 32% [Refs. 15, 16]. The data of Gilbert [Ref. 15] are included and show good agreement midway up the fountain, but poorer agreement at the bottom and top. It is likely that measurement errors (hot wire anemometry) are significant at the bottom and that simulation errors are significant at the top. The fountain must eventually relax to a conventional plane jet, although this may be occurring too rapidly in the simulation. Turbulence near the top boundary is damped by the dissipative outflow boundary conditions and coarser grid spacing, which decreases the spreading rate. Large scale motions are also constrained by the periodi-

city condition because the width of the fountain near the top boundary is greater than the z-dimension of the physical domain (see Fig. 16).

Figure 10 gives the mean velocity profiles in the fountain at several heights. The fountain is not perfectly symmetric although it should be. The factors which contribute to this are non-symmetric truncation errors in the MacCormack algorithm and insufficient integration time. It should be noted that most experimental results show some asymmetry and, thus, the fountain may easily be disturbed from symmetric.

The streamwise normal stress is given in Figure 11. Data from physical experiments of Gilbert [Ref. 15], Kind [Ref. 16] and Saripalli [Ref. 6] are included. The "normal" plane free jet has been studied by Bradbury [Ref. 17] and his results are quite close to those of Gilbert. The simulated results are below those from Kind but generally above those of Gilbert. Also, a sharp dip in the stress is seen at the centerline in the present results and the results of Kind, but not in those of Gilbert or Saripalli.

Contour plots of some turbulence quantities are given in what follows. In these, the normalizing velocity scale is $\sqrt{2\Delta p}$, where Δp is the maximum pressure rise in the collision zone. This is approximately the maximum mean velocity of the colliding wall jets. The normalizing length scale is half of the width of the high pressure region. The time scale derived from the length and velocity scales is approximately the minimum time for fluid to transit through the collision zone. Figure 12 gives contour plots of the normal stresses. The maximum for $\overline{u'u'}$ is 0.28 (note these are lateral fluctuations with respect to the fountain), and is seen near the centerline in the upper half of the collision zone. This is the point where the wall jets collide after having been forced up and over the separation zone at the base of the fountain. It is also the region of maximum streamline curvature. The regions of maximum $\overline{v'v'}$ in the fountain are on both sides of the upwash and are in much the same regions as we expect for the shear stress. The regions of highest $\overline{u'u'}$ and $\overline{v'v'}$ do not overlap which suggests that an important mechanism may be the inter-component transfer from $\overline{u'u'}$ to $\overline{v'v'}$. The regions of highest $\overline{w'w'}$ are very near the wall at the base of the fountain and in the upper part of the fountain. However, $\overline{w'w'}$ is relatively large in all regions of turbulent flow and does not show the strong spatial variations displayed by $\overline{u'u'}$ and $\overline{v'v'}$.

The turbulent shear stress normalized on the local centerline velocity, including the SGS contribution, is given in Figure 13 at a few stations in the fountain. The SGS contribution to the shear stress is large in the wall jet (about 50%), but small (less than 10%) in the fountain. The maximum stress is predicted to be about 0.075, which is in reasonable agreement with the data of Saripalli, but is considerably higher than the value of 0.024 reported by Gilbert. The stress is roughly three times greater than the maximum shear stress of 0.022 in a "normal" planar jet [Ref. 17] and, therefore, consistent with the spreading rate which is three times greater than in the "normal" jet. Figure 14 gives the shear stress as a contour plot which shows regions of high stress in the fountain and along the edge of the separation bubble at the base of the turning region.

3.3 Instantaneous Flow Field

Flow visualization of the turbulence can provide insights that can never be gleaned from statistical data. The computer code is not currently capable of saving all of the time dependent information we desire; however, we can examine an instantaneous three-dimensional flow field and learn some important points about the fountain.

Figure 15 gives particle tracers started in the opposing wall jets of the instantaneous flow field. The tracers show a small amount of mixing, indicated by crossing paths, in the wall jets. In the fountain considerably more mixing occurs, especially for $y > 6$ which is the region of maximum spreading rate. A mechanism that appears to be important is this: Blobs of fluid with higher u' can penetrate through the mean centerline of the fountain. Once through the centerline the blob meets less resistance to its motion since it is moving into a weaker flow and no adverse pressure gradient. This blob now travels on a path that is very different from the mean flow, which gives high mixing and shear stress. Another feature of this figure is that the fountain is slightly tilted. The tilt might indicate a "turbulence" mechanism consisting of the fountain flapping back and forth. The tilt does appear in the mean particle paths (Fig. 8-c) which may indicate this is a problem of asymmetry induced by the numerics. It is also possible that a low frequency flapping motion of the fountain exists, which has not been removed by the time averaging; this would be difficult to study because of the long integration times required and the dependence on low frequency fluctuations of the inflow conditions.

Figure 16-a gives velocity vectors projected in the x-z plane in the fountain at y=12. This shows a region of fluid, denoted A, with a large negative u' component penetrating into relatively quiescent fluid. Mach number contours in the same plane, Figure 16-b, show that this is a region of high speed flow, indicating the vertical velocity is large as well (positive v'). Thus, this blob will contribute to negative $\overline{u'v'}$. There is also a region (B) where the fountain fluid appears to be ingulfing a large area of ambient fluid. This may be the remnant of an earlier high speed blob which is now "mushrooming out" and forming vortices similar to the starting vortices from a free jet.

The fluid interactions we have examined in this single "snapshot in time" indicate that the fountain turbulence has a large scale structure caused by the penetration of blobs of high speed fluid through the mean fountain centerline. Data at other times also show these phenomena. The evidence for a flapping motion is relatively weak. The next step is to examine the results in terms that are amenable to Reynolds-averaged turbulence modeling.

3.4 Turbulence Mechanisms

Evaluation of the mechanisms that contribute to the high turbulent stresses will be done within the framework of the Reynolds stress transport equations, which are given here in cartesian tensor notation.

$$\frac{D}{Dt}\overline{u_i'u_j'} = \underbrace{[-\overline{u_i'u_k'}\frac{\partial U_j}{\partial x_k} - \overline{u_j'u_k'}\frac{\partial U_j}{\partial x_k}]}_{I} \underbrace{- 2\nu\overline{\frac{\partial u_j'}{\partial x_k}\frac{\partial u_i'}{\partial x_k}}}_{II} + \underbrace{\overline{\frac{p'}{\rho}[\frac{\partial u_i'}{\partial x_j} + \frac{\partial u_j'}{\partial x_i}]}}_{III} \quad (4)$$

$$+ \underbrace{\frac{\partial}{\partial x_k}[-\overline{u_i'u_j'u_k'} + \nu\frac{\partial\overline{u_i'u_j'}}{\partial x_k} - \overline{\frac{p'}{\rho}(\delta_{jk}u_i' + \delta_{ik}u_j')}]}_{IV \quad V \quad VI}$$

The left hand side of Equation 4 represents the rate of change of the components of Reynolds stress along streamlines. In order, the right hand side terms represent: production, viscous dissipation, pressure strain, turbulent diffusion, viscous diffusion and pressure diffusion. The terms which are thought to be major ones will be given as contour plots. Identical contour levels and normalization are used for all terms so that valid comparisons of the terms can be made from these figures. Only resolvable turbulence contributes to these results; the SGS shear stress is not included.

The production term is important because it extracts energy from the mean flow and converts it to turbulence. The pressure-strain term cannot produce turbulence energy; it merely transfers energy among the different components. Pressure-strain interactions can affect the shear stress by changing the correlation between u' and v'. The objective in this examination is to determine which are the principal terms in the generation of the high shear stresses.

The production term for $\overline{u'v'}$ is given in Figure 17-a. Regions of high production are seen at the separation bubble at the base of the fountain and in the fountain and are nearly coincident with the regions of high shear stress given in Figure 14. Figure 17-b gives the pressure-strain term for $\overline{u'v'}$ and shows levels comparable to the production term, but in different locations. The highest levels are where the wall jets first separate and there are moderate levels near to, but on either side of, the fountain centerline. The production and pressure-strain terms have, locally, the same sign in most of the flow and combine to increase the level of shear stress. It appears that the pressure-strain term is more important at the base of the fountain but the production term is more important in the fountain.

The gain or loss of $\overline{u'v'}$ due to turbulent diffusion, term IV, is given in Figure 17-c. Gradient diffusion models are typically used to model the velocity triple correlations, [Ref. 18], which for this flow means that regions with the largest stress would experience the greatest loss in much the way heat diffuses. Comparison of Figures 17-c and 14 suggests that the gradient diffusion concept is correct near the outer edges of the fountain, but not in the central region of the fountain, between the points of maximum shear stress magnitude. Term IV is only slightly less in magnitude than the production or pressure-strain, and therefore relatively important.

For the normal stresses a clear picture emerges regarding the roles of the different terms. Figures 18-a and 19-a show the production of $\overline{u'u'}$ and $\overline{v'v'}$. Production of $\overline{u'u'}$ occurs primarily at the collision point; this is where the mean flow is redirected upward, but the higher speed blobs penetrate through the mean centerline. The primary contributor to this term is $\overline{u'u'}$ dU/dx, which is large because dU/dx is so large. Production of $\overline{v'v'}$ occurs mainly in the fountain where $\overline{u'v'}$ dV/dx is large. There is a region of negative production of $\overline{v'v'}$ at the base of the fountain; negative production is impossible to obtain with a positive definite eddy viscosity model. The pressure strain terms for $\overline{u'u'}$ and $\overline{v'v'}$, given in Figures 18-b and 19-b, are of comparable magnitude, but opposite sign, in the collision zone; this indicates a transfer of energy from $\overline{u'u'}$ in the wall jet to $\overline{v'v'}$ in the fountain (note that v' is streamwise in the fountain).

4. SUMMARY

Numerical simulations with the three-dimensional Navier-Stokes equations were used to study turbulence mechanisms in a VTOL upwash fountain. The primary characteristic of this flow, the abnormally high spreading rate of the fountain, was predicted. Large values of the Reynolds stresses were also predicted and these are in moderately good agreement with the (widely scattered) experimental data. The pressure-strain and production terms in the Reynolds shear stress transport equation have been compared and are shown to be of comparable magnitude and of the same sign. The principal mechanism for generating the high shear stress is the penetration of blobs of high speed fluid through the mean fountain centerline. This is reflected in the large magnitudes of the production terms for the lateral fluctuations ($\overline{u'u'}$) and the shear stress ($\overline{u'v'}$).

This is a flow for which advanced turbulence models have failed to give good results. The success of very large eddy simulation for what could be described as an engineering application may point the way for the prediction of other difficult turbulent flows.

The authors gratefully acknowledge the support of the Air Force Office of Scientific Research, External Aerodynamics, through contract No. F49620-85-C-0055, and the NASA Ames Reseach Center for use of the CRAY computer.

REFERENCES

1. Gillis, J. C. and Johnston J. P., "Turbulent Boundary Layer Flow and Structure on a Convex Wall and its Redevelopment on a Flat Plate," J. Fluid Mech. 135, pp. 123-153, 1983.

2. Bradshaw, P. and Castro, I. P., "The Turbulence Structure of a Highly Curved Mixing Layer," J. Fluid Mech. 73, part 2, pp. 265-304, 1976.

3. Moser, R. D. and Moin, P., "Direct Numerical Simulation of Curved Turbulent Channel Flow," Stanford Univ. Mech. Engrg. Thermo. Div. Rept. TF-20, 1984.

4. Childs, R. E. and Nixon, D., "Simulation of Impinging Turbulent Jets," AIAA-85-0047.

6. Saripalli, K. R., "Laser-Doppler-Velocimeter Measurements in a Three-Dimensional Fountain Upwash," to be presented at the AIAA/AHS/ASEE Aircraft Design, Systems and Operations Meeting, Colorado Springs, CO, Oct. 1985.

7. Rogallo, R. S. and Moin, P., "Numerical Simulation of Turbulent Flows," Ann. Rev. Fluid Mech. 16, pp. 99-137, 1984.

8. MacCormack, R. W., "A Numerical Method for Solving the Equations of Compressible Viscous Flow," AIAA-81-0110.

9. MacCormack, R. W., "Current Status of Numerical Solutions of the Navier-Stokes Equations," AIAA-85-0032.

10. Reynolds, W. C., "Computation of Turbulent Flows," Stanford Univ. Mech. Engrg. Thermo. Div. Rept. TF-4, 1975.

11. Moin, P., Reynolds, W. C., Ferziger, J. H., "Large Eddy Simulation of Incompressible Turbulent Channel Flow," Stanford Univ. Mech. Engrg. Thermo. Div. Rept. TF-12, 1978.

12. Yee, H. C., "Numerical Approximations of Boundary Conditions with Application to Inviscid Equations of Gas Dynamics," NASA TM-81265, 1981.

13. Boris, J., Oran, E., Grinstein, F., Oswald, C., and Gardner, J., "Direct Simulations of Spatially Evolving Compressible Turbulence: Techniques and Results," presented at Ninth International Conference on Numerical Methods in Fluid Dynamics, CEN - Saclay, France, June 1984.

14. 1980-81 Stanford-AFOSR-HTTM Conference on Complex Turbulent Flows, S. J. Kline et al., Eds., Stanford, CA, 1981.

15. Gilbert, B. L., "An Investigation of Turbulence Mechanisms in V/STOL Upwash Flow Fields," Grumman Aerospace Corp. Rept. RE-688, 1984.

16. Kind, R. J. and Suthanthiran, K., "The Interaction of Two Opposing Plane Turbulent Wall Jets," AIAA-72-0211.

17. Bradbury, L. J. S., "The Structure of a Self-Preserving Turbulent Plane Jet," J. Fluid Mech. 23, part 1, pp. 31-64, 1965.

18. Launder, B. E., Reece, G. J, and Rodi, W., "Progress in the Development of a Reynolds-Stress Turbulence Closure," J. Fluid Mech. 68, part 3, pp. 537-566, 1975.

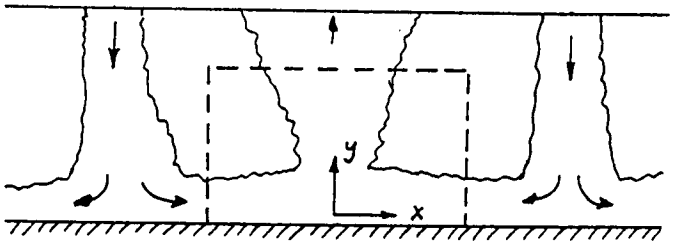

Figure 1. Sketch of impinging jets with upwash fountain, showing computational domain.

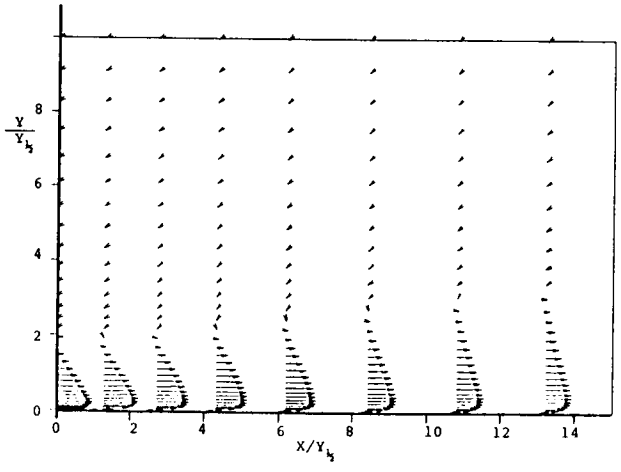

Figure 2. Time averaged velocity vectors in wall jet.

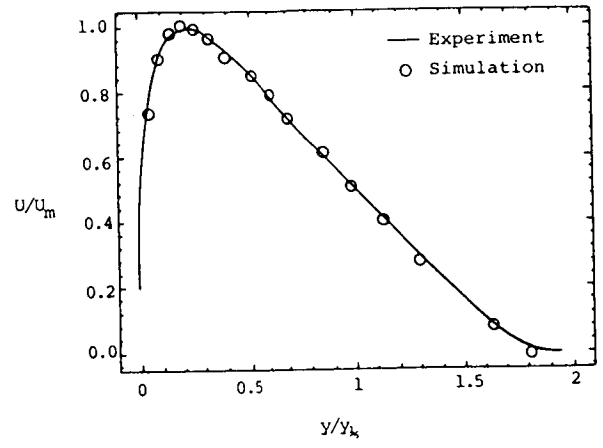

Figure 3. Comparison of velocity profile at x=10 with experimental data from Ref. 14.

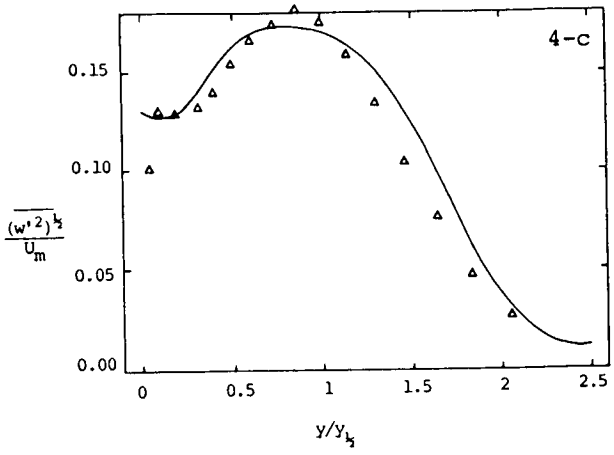

Figure 4. Normal stresses in the wall jet: a) gives u´; b) gives v´; c) gives w´.

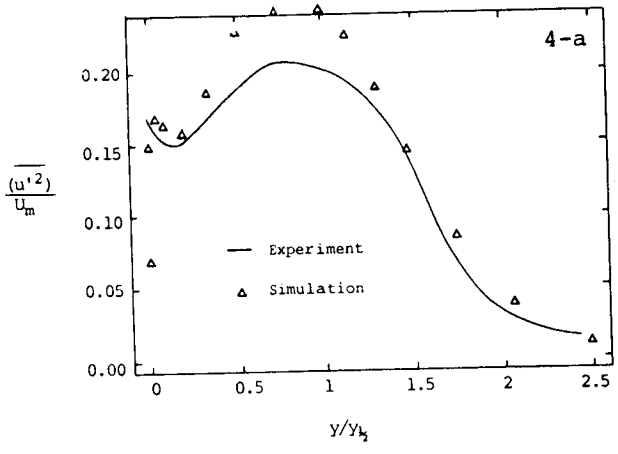

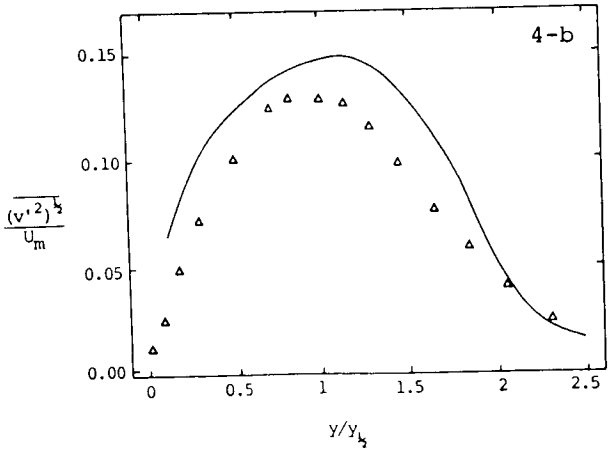

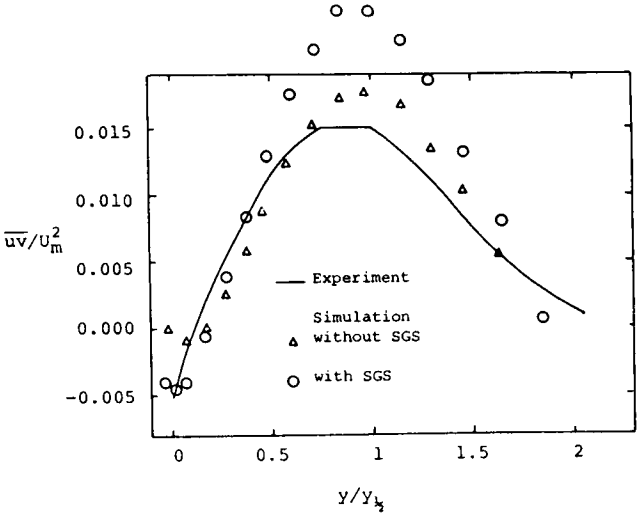

Figure 5. Shear stress in the wall jet, with and without sub-grid-scale contribution.

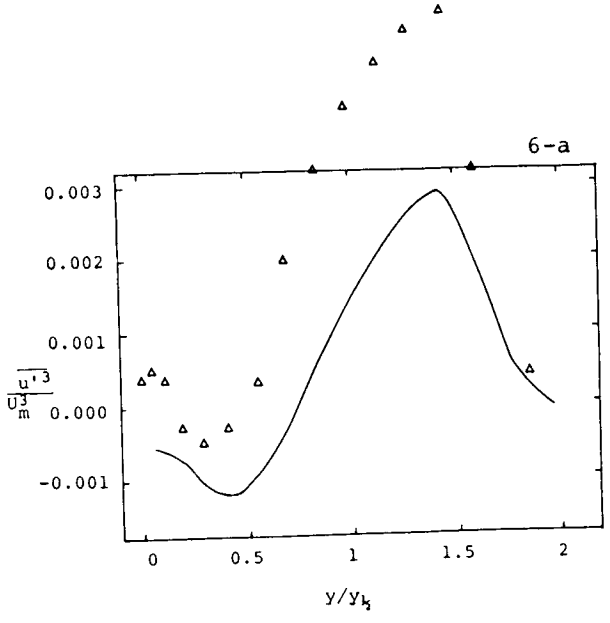

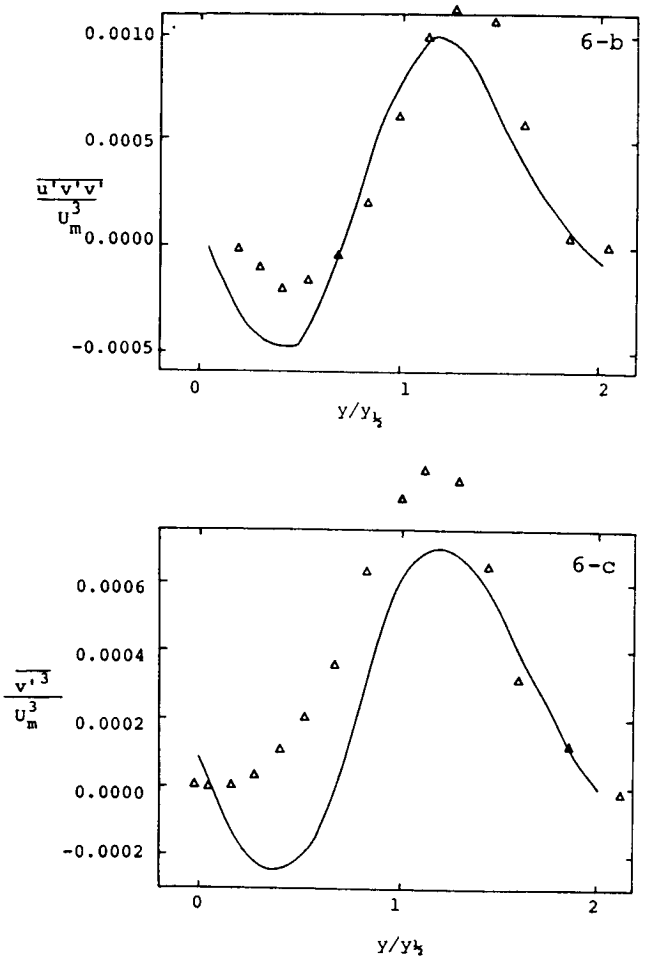

Figure 6. Triple velocity correlations in the wall jet: a) gives $u'u'u'$; b) gives $u'u'v'$, c) gives $v'v'v'$.

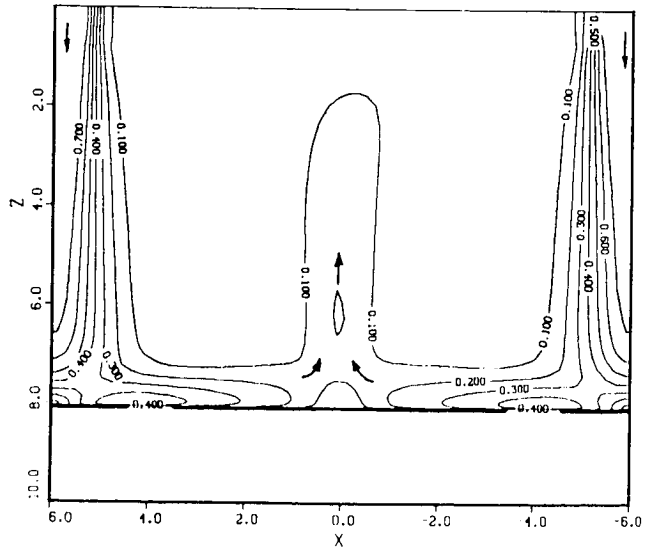

Figure 7. Mach number contours from a steady state k-ε calculation, which underpredicts the fountain spreading rate, from Ref. 5.

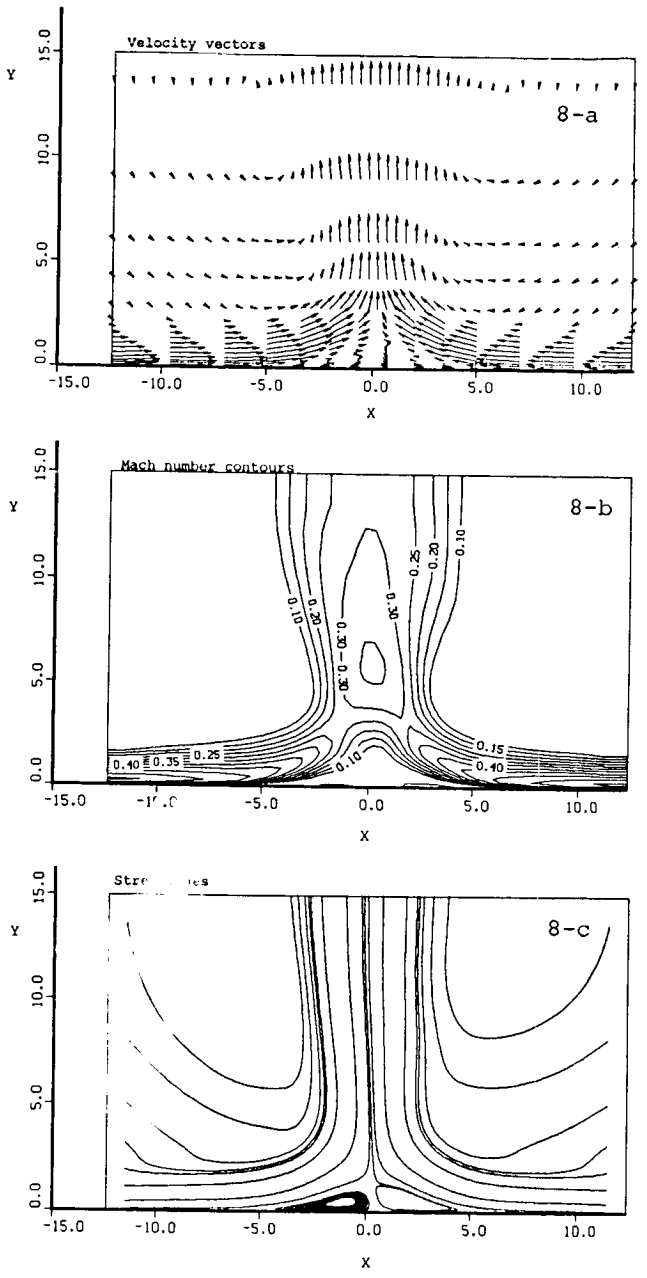

Figure 8. Mean results from unsteady fountain simulation: a) give velocity vectors; b) gives Mach number contours; c) gives streamline which show separation at base of fountain.

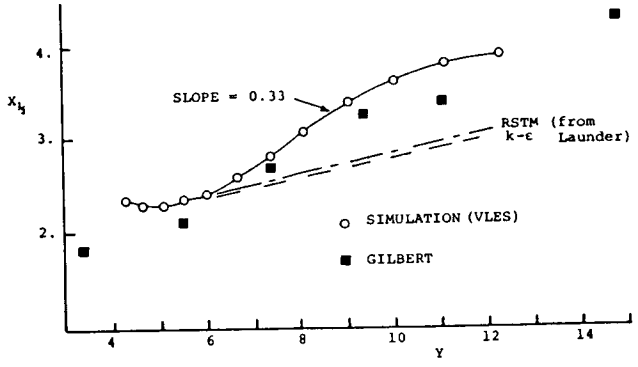

Figure 9. Half velocity width spreading rate in the fountain and comparison with data from Gilbert, Ref. 15.

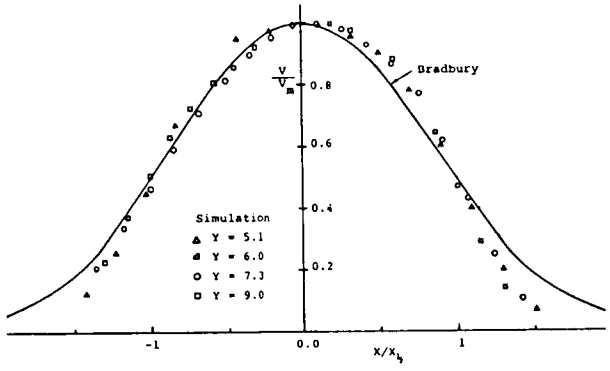

Figure 10. Mean velocity profiles in the fountain and comparison with "normal" plane jet, Ref. 17.

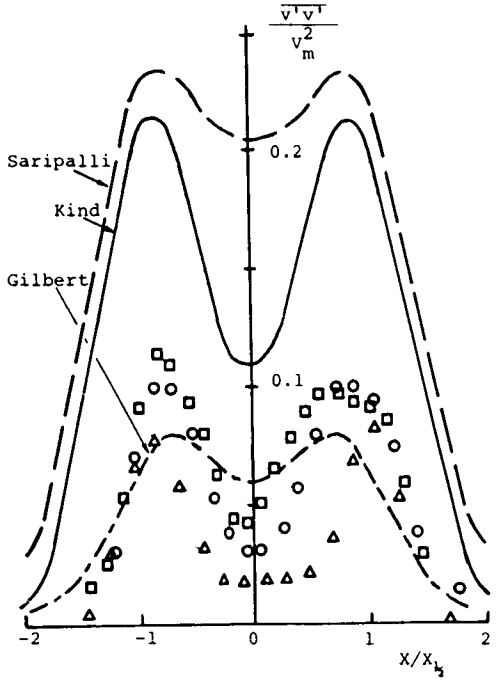

Figure 11. Streamwise normal stress, $\overline{v'v'}$, , in the fountain, comparison with Refs. 15 and 16; see Figure 10 for symbols.

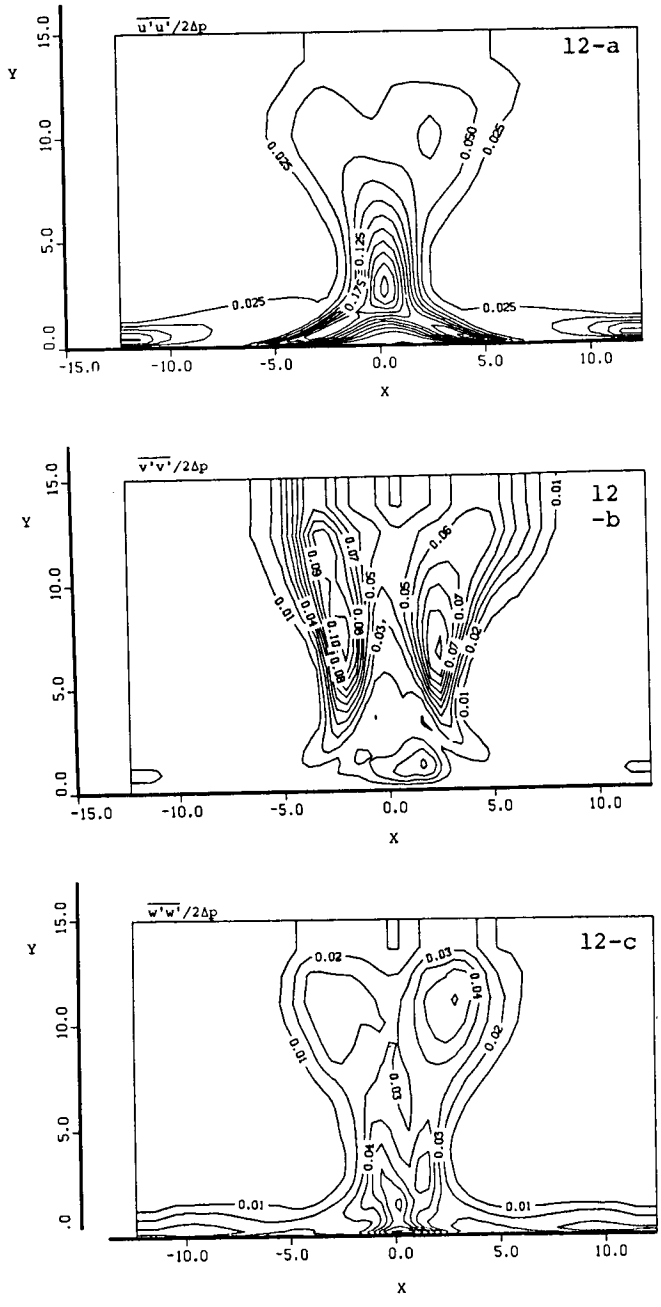

Figure 12. Contour plots of normal stresses: a) gives u´u´; b) gives v´v´; c) gives w´w´.

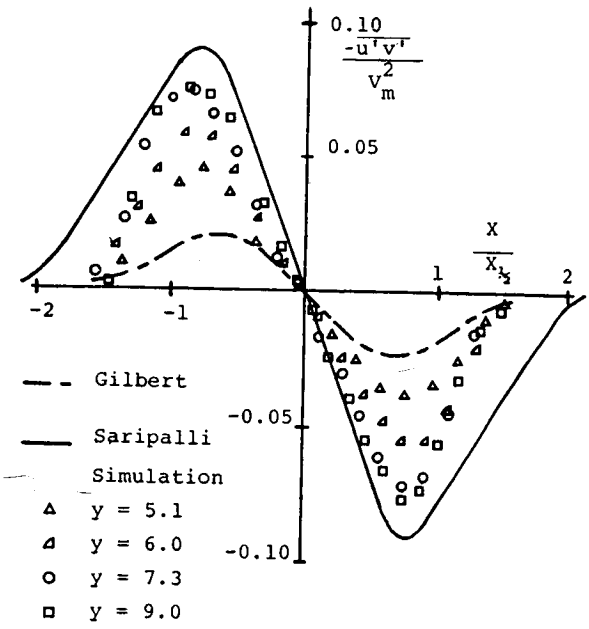

Figure 13. Shear stress in the fountain.

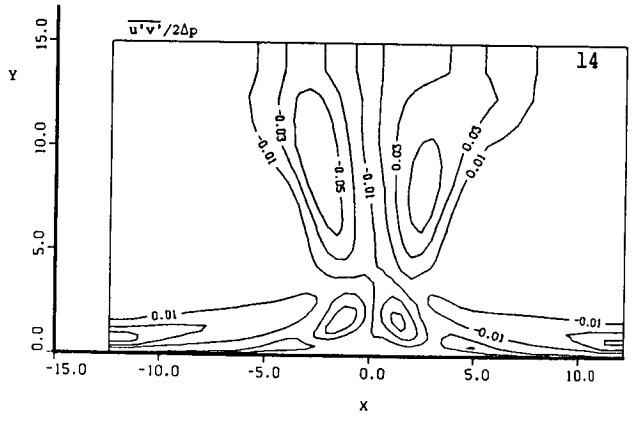

Figure 14. Contour plot of the shear stress, including SGS stress.

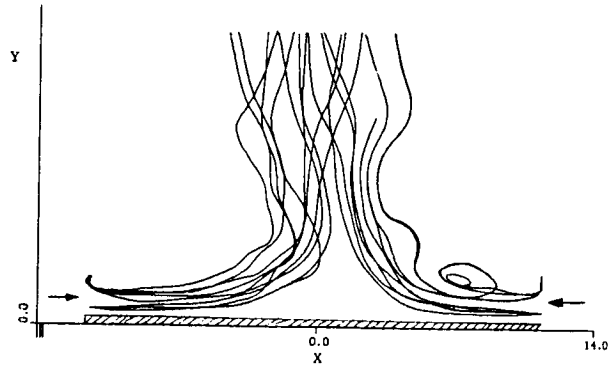

Figure 15. Tracer particles in an instantaneous flow field (see text).

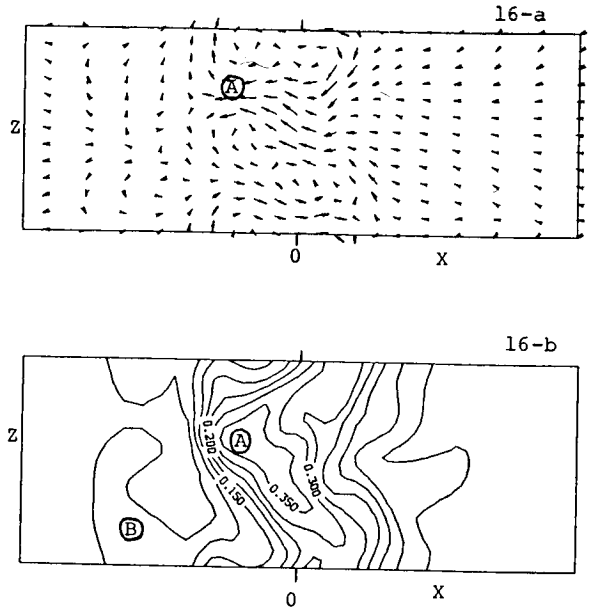

Figure 16. Instantaneous flow field in the fountain on a plane normal to the streamwise direction: a) gives velocity vectors; b) gives Mach number contours.

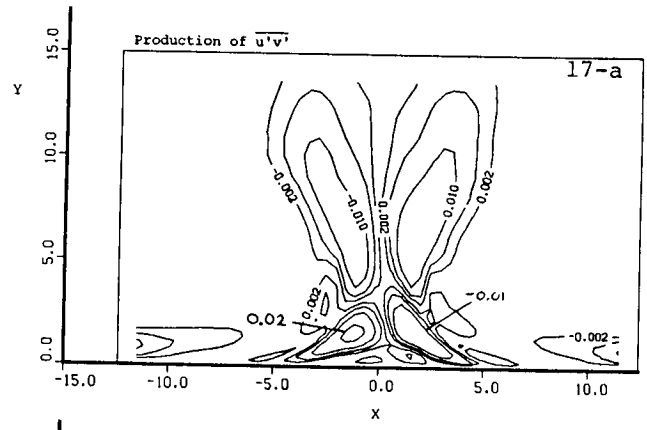

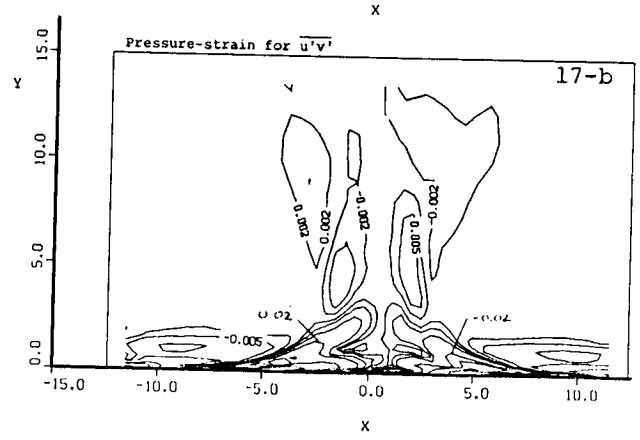

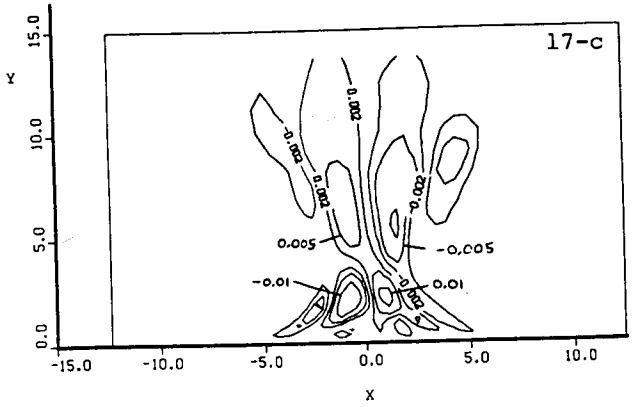

Figure 17. Terms in the Reynolds stress transport equation for $\overline{u'v'}$: ; a) production; b) pressure-strain; c) net gain or loss due to turbulent transport (term IV).

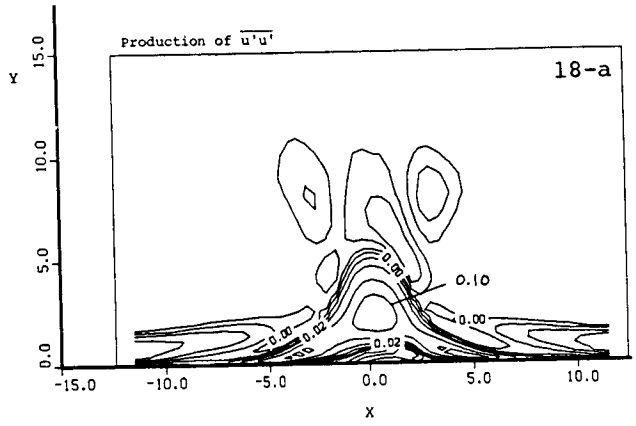

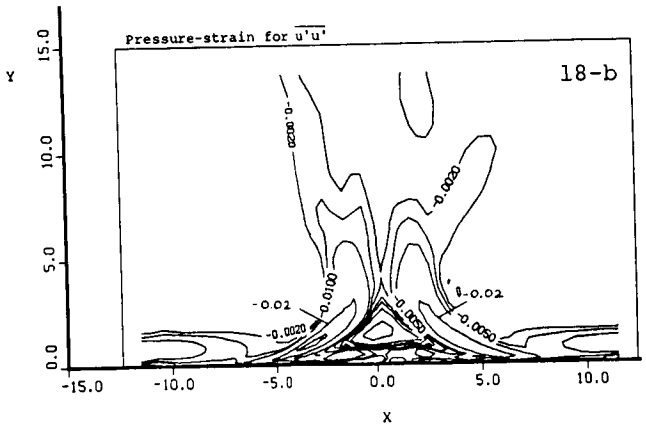

Figure 18. Terms in the Reynolds stress transport equation for $\overline{u'u'}$: a) production; b) pressure-strain.

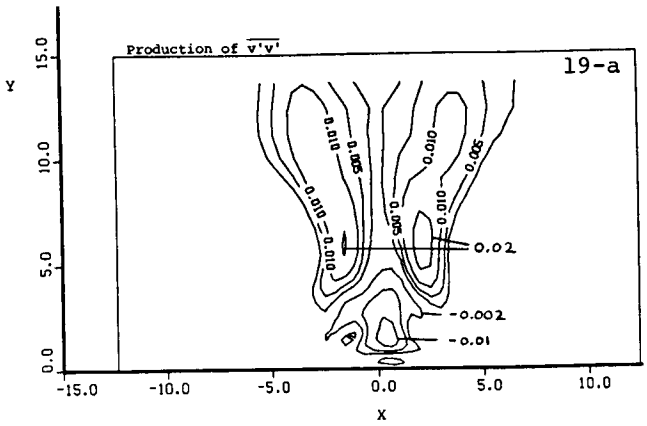

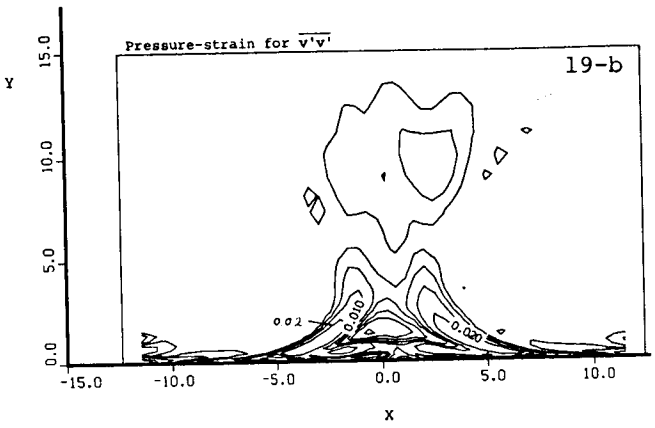

Figure 19. Terms in the Reynolds stress transport equation for $\overline{v'v'}$: a) production; b) pressure-strain.